PAPER

A prospect of cost-effective handling and transportation of graphene oxides: folding and redispersion of graphene oxide microsheets

To cite this article: Chao-Wen Chang et al 2021 Nanotechnology 32 455601

View the article online for updates and enhancements.



IOP Publishing Nanotechnology

Nanotechnology 32 (2021) 455601 (11pp)

https://doi.org/10.1088/1361-6528/ac1755

A prospect of cost-effective handling and transportation of graphene oxides: folding and redispersion of graphene oxide microsheets

Chao-Wen Chang^{1,4}, Somayeh Zamani^{1,4}, Detlef M Smilgies¹, Honguk Seo², Sangjoon Park², Taechung Kang², Ae Ran Lim³ and Yong Lak Joo^{1,*} ®

E-mail: ylj2@cornell.edu

Received 8 April 2021, revised 12 July 2021 Accepted for publication 23 July 2021 Published 17 August 2021



Abstract

Controlling the assembly of 2D materials such as graphene oxides (GO) has a significant impact on their properties and performance. One of the critical issues on the processing and handling of GO is that they need to be in dilution solution (0.5 to 2.5 wt%) to maintain their high degree of exfoliation and dispersion. As a result, the shipment of GO in large quantity involves a huge volume of solvent (water) and thus the transportation costs for large sales volume would become extremely high. Through cross-sectional scanning electron microscopy and polarized optical microscopy together with x-ray diffraction and small-angle x-ray scattering studies, we demonstrated that the assembly and structure of GO microsheets can be preserved without restacking, when assembled GO via water-based wet spinning are re-dispersed into solution. A couple of alkyl ammonium bromides, CTAB and TBAB, as well as NaOH, were examined as coagulants and the resulting fibers were redispersed in an aqueous solution. The redispersed solution of fibers that were wet-spun into the commonly used CTAB and TBAB coagulation baths, maintained their physico-chemical properties (similar to the original GO dispersion) however, did not reveal preservation of liquid crystallinity. Meanwhile, the redispersed fibers that were initially spun into NaOH coagulation bath were able to maintain their liquid crystallinity if the lateral size of the GO sheets was large. Based on these findings, a costeffective solid handling approach is devised which involves (i) processing GO microsheets in solution into folded layers in solid-state, (ii) transporting assembled GO to the customers, and (iii) redispersion of folded GO into a solution for their use. The proposed solid handling of GO followed by redispersion into solution can greatly reduce the transportation costs of graphene oxide materials by reducing the transportation volume by more than 90%.

Keywords: transportation, redispersion, folded layers, graphene oxide, liquid crystal, SAXS

1

(Some figures may appear in colour only in the online journal)

¹ School of Chemical and Biomolecular Engineering, Cornell University, Ithaca, NY 14853, United States of America

²Research Institute of Chemistry, JMC Corp., Ulsan, 44998, Republic of Korea

³ Department of Carbon Convergence Engineering and Department of Science Education, Jeonju University, Jeonju 55069, Republic of Korea

⁴ Co-first authors: Chao-Wrn Chang and Somayeh Zamani.

^{*} Author to whom any correspondence should be addressed.

1. Introduction

Since its discovery in 2004, the interest in free-standing, monolayer graphene has continuously increased. The exceptional electrical, thermal and mechanical properties of these 2D planar sheet comprising sp²-bonded carbon structure, makes it promising for potential applications such as lightweight materials, sensors, and energy-related materials. Obtaining pristine graphene, however, is very challenging due to its poor solubility and processability [1, 2]. While there has been the development of graphene via direct exfoliation of graphite [3], a naturally occurring mineral, chemical reduction of graphene oxide (GO) through strong oxidation of graphite, is one of the most common methods to produce graphene-like monolayers [4-6]. GO sheets bearing myriad oxide functionalities in the form of alcohols and epoxides possess expanded layer distance and hydrophilic surface [7]. It can practically be deposited on any substrate and then be reduced to conductive graphene [8, 9]. For this specific reason, GO is used in the production of transparent conductive films applicable in flexible electronics [10], chemical sensors, etc [11]. Some other applications include chemical catalysis [12, 13], and water and wastewater treatments [14–16]. Due to its high surface area, GO is also used as electrode materials in batteries [17–21], capacitors, and solar cells [22, 23].

Despite its advantages and industrial applications, Go transportation still confronts challenges. To maintain the exfoliation state of the sheets, GO is remained dispersed in a dilute aqueous solution and the concentration is usually in the range of 0.05–2 wt.% [2, 24, 25]. A shipment of 5 kg GO, for example, requires transportation of at least 250 liters of water. Such significant cost on water transportation is not reasonable and novel transportation approaches to avoid this cost are highly demanded. Additionally, considering the toxicity of GO, there have been increasing concerns over its accidental release into the environment and the living system [26–28]. Therefore, transportation of GO in ways other than the solution form is an urgent concern for the industry.

We propose here, a novel transportation form of self-assembled GO fibers to overcome the abovementioned challenge. It implements the cost-effective, fast, and easy to scale-up method of wet spinning process [29] to assemble GO particles into layered fibers. The presence of a small amount of coagulation agent in a bath results in compact fibers or platelets forming immediately soon after extruding pristine GO gel solution. In this case, when GO is transported in the solid form of fibers, the largely reduced volume due to the elimination of the use of solvent will dramatically bring down the cost. Solid fiber is also much easier to manage than gel solution, and this could further prevent GO from leaking into the environment and harm living organisms. The challenge is whether these fibers can be re-dispersed back into water and maintain the chemical and physical properties of the original solution and whether the water dispersion retains the important liquid crystallinity. To this aim, comprehensive characterization of assembled GO microsheets via wet-spinning into different coagulation baths was conducted, followed by redispersion into water. We demonstrate that the folded structure of GO in the fiber form and thus re-dispersion capability and preservation of liquid crystal state after re-dispersion depends on the coagulant, and the re-dispersion state of GO can be tailored by the proper selection of the coagulation agent.

2. Experimental methods

2.1. Materials

GO aqueous solution was purchased from EMD Performance Materials Corp. and JMC-KISCO Co. Hexadecyltrimethylammonium bromide (CTAB) (>98%) and Tetrabutylammonium bromide (TBAB) were purchased from Sigma-Aldrich. Sodium hydroxide (pellets) was purchased from Mallinkrodt Chemicals. Ethyl alcohol (>99%) was obtained from VWR Chemicals.

2.2. GO fiber fabrication

The GO dispersion from EMD (as it is received, 2 wt.% in water) was sonicated for 30 min to degass the dispersion, and loaded in a plastic syringe (Luer Lock VWR syringe, 5 ml)., The dispersion was injected into a coagulation bath that was rotating (15 rpm). The infusion rate was 0.5 ml min⁻¹ and the coagulation bath consisted of NaOH (1 mg ml⁻¹), CTAB (0.5 mg ml⁻¹), or other coagulant solutions in a 1:1 volume ratio of water and ethanol. The obtained fibers remained in the NaOH or CTAB bath for 10 or 30 min respectively, followed by winding the fiber around a Teflon bar. The Teflon bar was then soaked in a washing bath (1:1 volume ratio of water and ethanol) for another 30 or 60 min. The fibers then were unwounded from the Teflon bar and dried at room temperature after taking out from the bath.

2.3. Redispersion in aqueous media

The fibers were ground into powder using a mortar and pestle. To Check the re-dispersion of GO powders, the powdered GO was then dispersed in water (2 wt.%) by 30 s of vortex mixing and 3 h of sonication bath. GO-CTAB samples underwent 3 min of further ultra-sonication to obtain a uniform dispersion.

2.4. Characterization methods

Fiber morphology was characterized by field-emission scanning electron microscope (SEM) LEO (Zeiss) 1550. Energy dispersive x-ray images were taken on the same SEM instrument. X-ray diffraction (XRD) patterns were determined by a D8 Advance ECO powder diffractometer (Bruker Corporation) using a high-brilliance 1 kW x-ray source. Scienta Omicron ESCA-2SR with operating pressure ca. 1×10^{-9} mBar was used to analyze the GO fibers by x-ray Photoelectron Spectroscopy (XPS). Measurement condition was according to previously reported method [30]. The Fourier transformed infrared spectrum was measured with a PerkinElmer Frontier MIR Spectrometer coupled with a LiTaO₃ MIR detector in the range of 600–4000 cm⁻¹ with 32 scans for each sample. Optical microscopy (OM) was utilized by an Amscope 40-1000× binocular compound microscope with

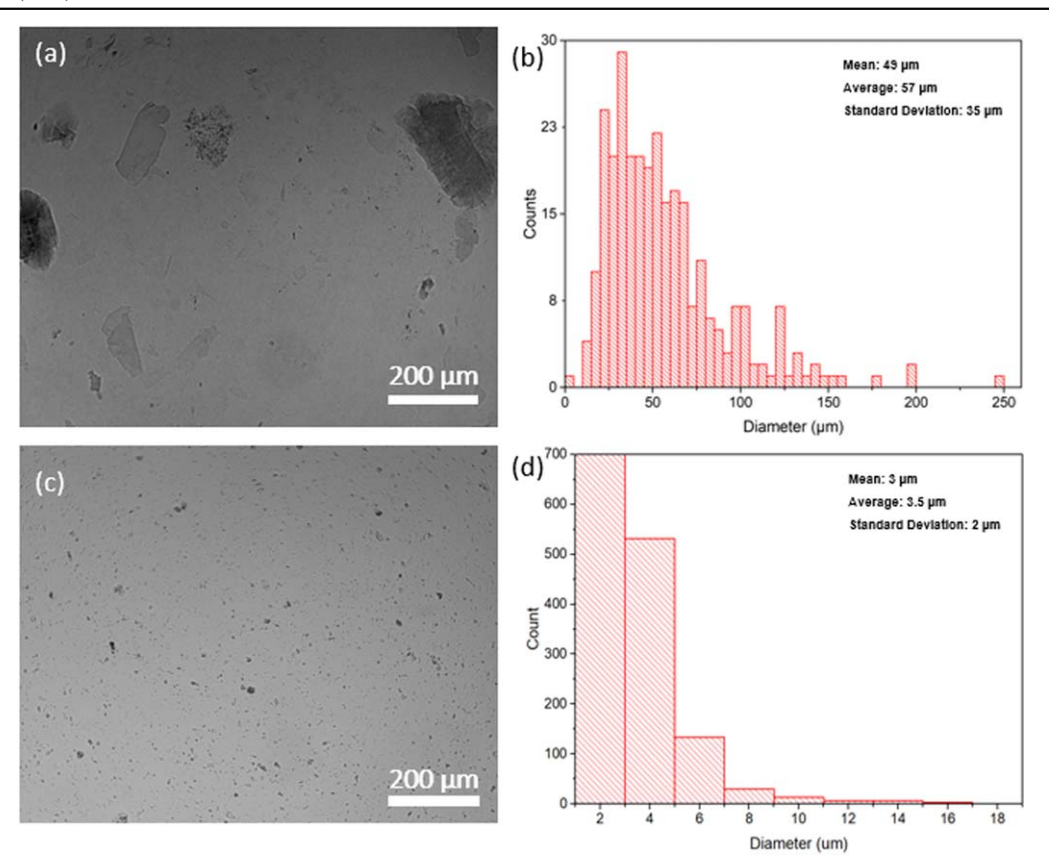


Figure 1. (a) Optical microscope images of LGO pristine gel solution and (b) particle lateral size distributions. (c) Optical microscope images of SGO pristine gel solution and (d) particle lateral size distributions.

a digital camera. Polarized optical microscopy (POM) was conducted using Olympus BX51 with a cross-polarization filter with a rotating stage. Additional TBAB coagulation agent, which is chemically similar to CTAB but with shorter carbon chains, was examined to compare with other cases. Zeta potential measurements were obtained by Zetasizer Nano ZS, Malvern. For this purpose, Sodium hydroxide (10 wt.%) was used for a rapid pH adjustment to titrate pristine JMC 40 GO gel solution along with 1 wt.% sodium hydroxide for precise control. The solution was adjusted to pH = 11. small-angle x-ray scattering (SAXS) measurements were performed at beamline ID3B at the Cornell High Energy Synchrotron Source. The Incident beam size was $0.1 \text{ mm} \times 0.1 \text{ mm}$ at a beam energy of 9.7 keV. For the measurements, GO solutions (including GO-TBAB) were filled into thin-walled glass capillaries (Charles Supper Inc.). Scattering signals were detected with a Pilatus3 300 k detector (Dectris) with a pixel size of 0.172 mm and at a distance of 2382 mm from the sample. Solutions were probed at 2 or 3 spots, 1 mm apart from each other, along the center of the capillary.

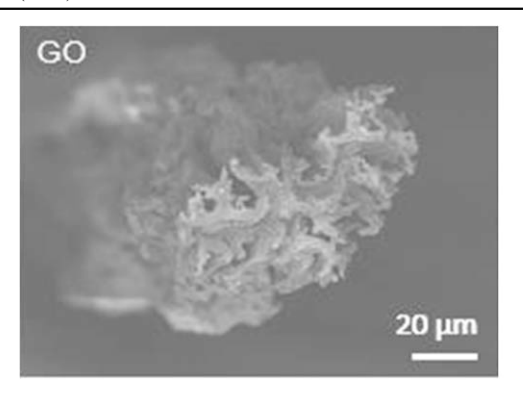
3. Results and discussion

Two different GO sources were used to show the influence of the sheet size, 2 wt.% GO gel solution provided by EMD Performance Material Co. and another one by JMC Corp. The main difference between the two GO solutions is in their lateral size. It has been reported in the literature that the lateral size of the GO sheets is directly correlated to the fiber properties [31]. Due to lower bending modulus in large size GO sheets, fibers are fabricated easier and stronger than the case with small size sheets [32].

Both solutions were well dispersed in water and possessed a similar degree of oxidization. GO provided by EMD had an average lateral size of 57 μ m, 10 times larger than that provided by JMC Corp. Accordingly, EMD GO is named as large GO (LGO), and JMC GO is called small GO (SGO). OM images and particle lateral size distributions of LGO and SGO solutions used in the study are illustrated in figure 1.

Cetyltrimethylammonium Bromide (CTAB) is one the most common coagulants for graphene-based materials in wet-spinning and we have previously shown that it is an effective coagulant to fabricate graphene and GO fibers [3, 30], therefore it was used as the first coagulant in this work. During the wet-spinning process into a bath with a charged coagulant such as CTAB, GO sheets are confined within the syringe tip and the needle. When encountering CTAB molecules, charge neutralization leads to hydrophobic–hydrophobic interactions to dominate and curling and folding of the GO sheets occurs. The right SEM image in figure 2, reveals the extremely compact folding of the LGO sheets after wet spinning, followed by coagulation with CTAB. It should be noted that GO sheets with large lateral sizes are folded compactly and form a fiber with a unique morphology.

Elemental percentages of the LGO and SGO fibers were determined through XPS measurements. The data are presented



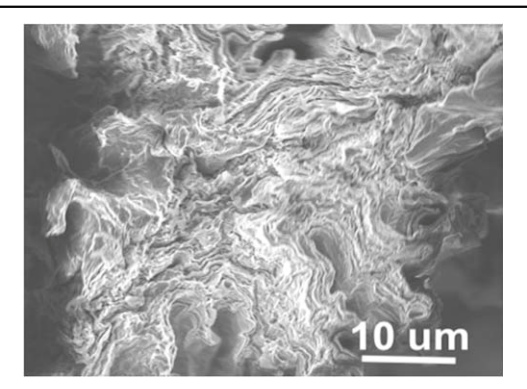


Figure 2. Cross-sectional SEM images of LGO fibers.

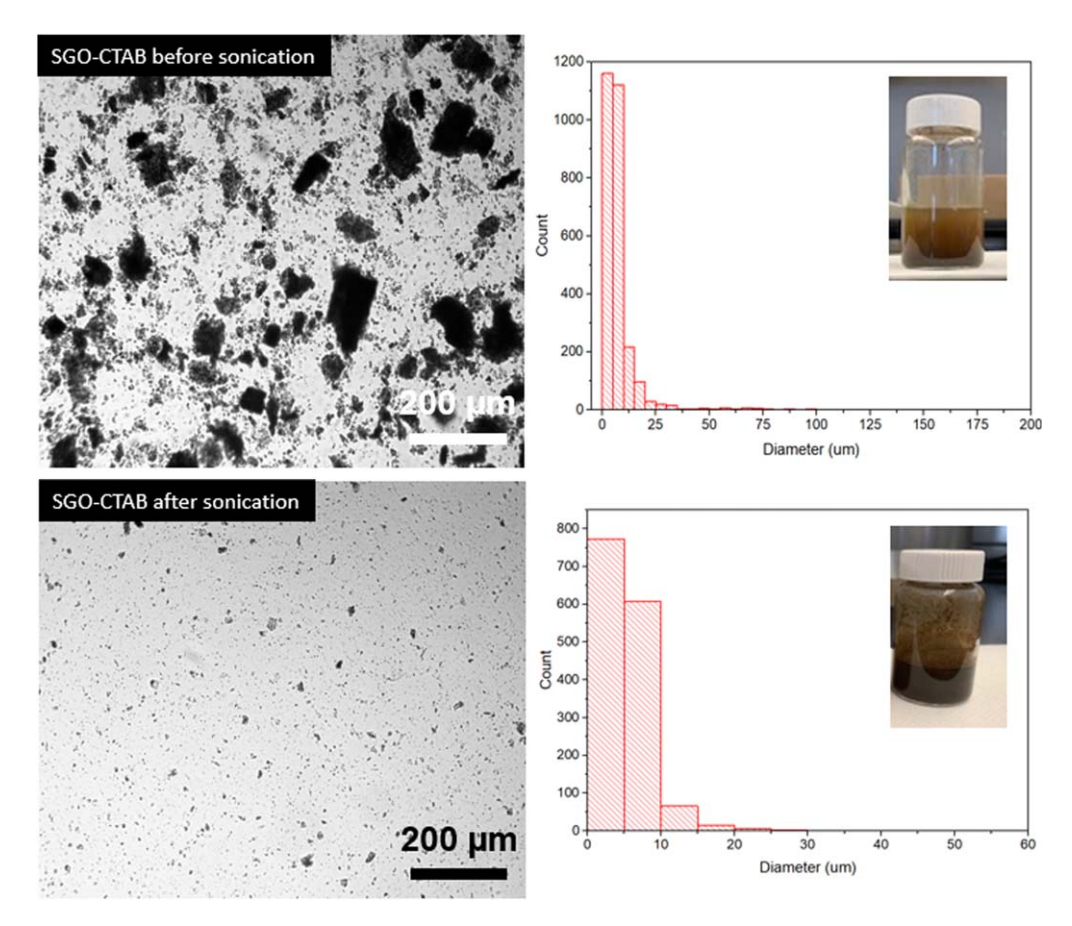


Figure 3. Optical microscope images of SGO-CTAB fiber dispersed in water and particle lateral size distributions. The top and bottom are before and after sonication/ultra-sonication respectively. The scale bar is $200 \mu m$.

in figure S1 (available online at stacks.iop.org/NANO/32/455601/mmedia). The percentage of C and O was 64.8 and 68.8%, and 30.9 and 31.2% in LGO and SGO, respectively. The O% and C% of the SGO sample were confirmed by EDS measurement while SEM was utilized (figure S1).

3.1. Conformation and characterization

The GO fibers were then re-dispersed back into the water to obtain GO-CTAB solution on which, chemical and physical properties characterization were conducted and compared to those of the original GO solution. We will use 'GO-coagulant' as the name of fiber redispersion samples.

Figure 3 shows the image of the re-dispersed SGO-CTAB fiber in water with and without sonication. Ultra-sonication drastically facilitated the dispersion of GO and decreases the average lateral size of the GO sheets. Before ultra-sonication, the large agglomerates precipitated within 5 min. After ultra-sonication for 3 min, the slurry was well dispersed in water even after resting for a day. The sonicated dispersion of GO particles still looked opaque.

It is well known that although GO sheets are highly dispersed in the GO solution, interestingly, even after the GO solution is dried, water molecules remain stuck in the GO powder via hydrogen bonding interactions between water molecules and oxygen-containing functional groups of GO.

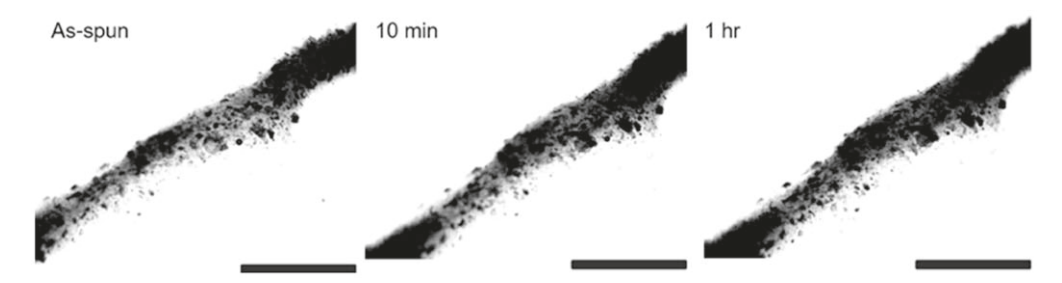


Figure 4. Optical microscopy images of LGO gel-like fiber in 1 wt.% NaOH coagulation bath (scale bar is 500 μ m).

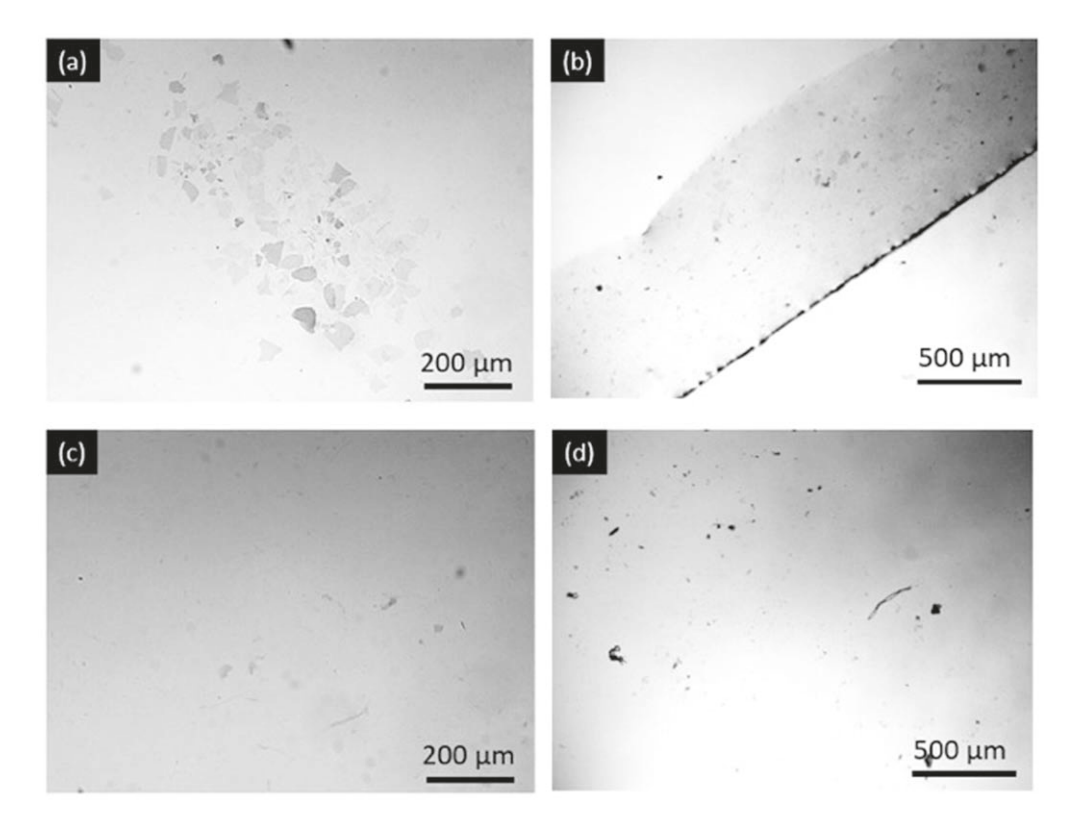


Figure 5. Optical microscope images of water re-dispersion of LGO-NaOH fiber. The gel fibers were immersed in 1 wt.% NaOH coagulation bath for (a), (b) 10 min and (c), (d) 30 min.

These water molecules are often referred to as 'intercalated' water molecules [33, 34]. The intercalated water molecules play a decisive role in the restacking of GO sheets as the hydrogen bonding facilitates interactions between GO sheets, resulting in aligning the GO sheets in the same orientation. Herein, from the optical microscopy images, the particles remain black even after ultra-sonication. We assume that CTAB is a strong coagulation agent which helps GO sheets aggregate easily. Hydrogen bonding interactions and acidic environment facilitate GO stacking. Hence, the introduction of CTAB and water molecules may not be ideal for returning GO fibers to initial gel states after redispersion.

As a result, a weaker coagulant/better dispersant may be needed to reduce GO's strong tendency to agglomerate, while this chemical cannot be too weak to form stable GO continuous fibers. Several coagulation agents were examined to produce GO fibers. Triton X-100 and Sodium Cholate are two well-known surfactants, but unlike CTAB, they cannot form

structurally stable GO fibers and will decompose within a few minutes in the bath (figure S2). According to the literature, sodium and potassium hydroxide are weaker coagulants than alkaline earth salts [31]. Therefore, it was hypothesized that it is possible that sodium hydroxide can perform as a better coagulant to preserve GO conformation and even the liquid crystallinity of its gel solution after redispersion.

Figure 4 shows the images of an LGO fiber in NaOH coagulation bath. There is almost no conformation change of the GO sheets when the fibers formed in the NaOH bath even after 1 h of soaking time. However, when the dried LGO-NaOH fibers are redispersed, different soaking times resulted in different conformations.

Figures 5(a) and (b) showed flat and more transparent sheets; yet (c) and (d) revealed striped and distorted flakes. Less soaking time (i.e. 10 min) preserved the sheet conformation; that is, become less affected by the presence of NaOH. The variation of GO conformation directly affected

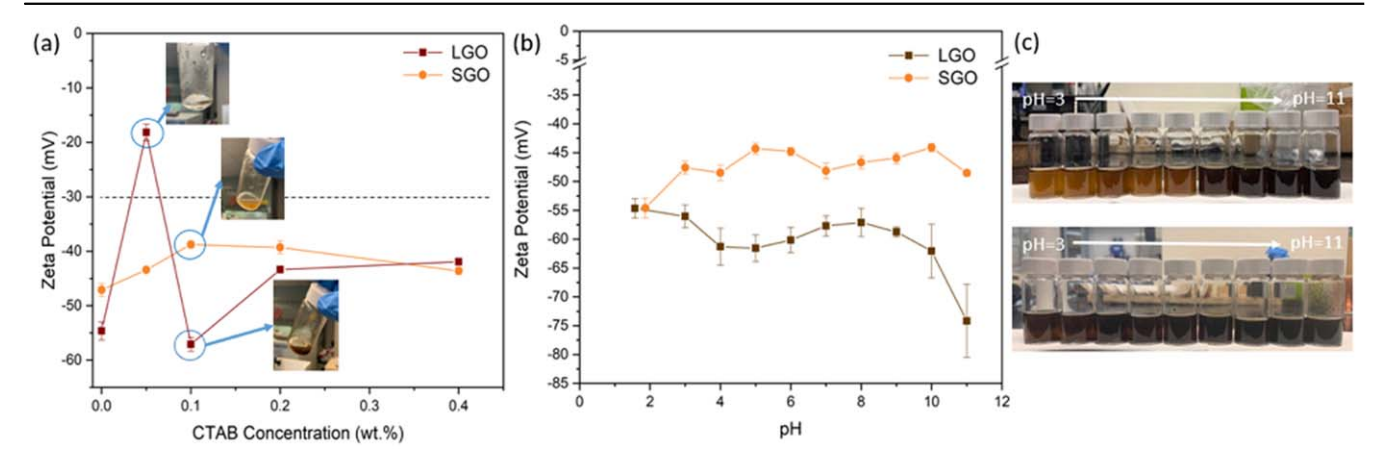


Figure 6. Zeta potentials for (a) LGO-CTAB and SGO-CTAB versus different CTAB coagulation bath concentrations and (b) LGO-CTAB and SGO-CTAB versus different pH values. NaOH was used for titration. (c) The photo shows LGO-CTAB and SGO-CTAB solutions after pH adjustment. The solution concentration is less than 1 wt.% adjustment to show color differences.

the solution viscosity. Lesser surface interaction between sheets resulted in lower viscosity if the sheets are more distorted. Fortunately, figures 5(a) and (b) manifest more complete and exfoliated sheets compared to figure 4. We conclude that sodium hydroxide is a better coagulant for preserving GO conformation after redispersion of GO fibers. This is also further proved by the morphology of the electrosprayed GO particles shown in figures S3 and S4.

To further our understanding of the relationship between the GO sheet surface properties in different coagulation media, the Zeta potential of two GO systems (LGO and SGO) was measured. Figure 6(a) represents the relationship between zeta potential and concentration of CTAB.

The 0.0 wt.% point represents the pristine GO gel solution and the other four points are solutions of redispersed GO fibers with different coagulant concentrations. It is well-known that GO can form well-dispersed aqueous colloids [35, 36].

Our study on the surface charge (zeta potential) of asprepared GO sheets shows that these sheets are highly negatively charged when dispersed in water (figure 6) due to the ionization/hydrolysis of O-groups, and GO zeta-potential can reach $\zeta=-60$ mV at pH 10. The stability of aqueous GO colloids was therefore attributed to electrostatic repulsion rather than hydrophilic interaction. The addition of NaOH coagulation solution causes GO to precipitate from the solution, due to salting-out effects. GO extracted from high pH solution and dried collapsed into star-like formation comprising several sheets or bundles [37].

Apparently, this is a consequence of the ionization of the carboxylic acid and phenolic hydroxyl groups that are known to exist on the GO sheet. This result suggests that the formation of stable GO colloids should be attributed to electrostatic repulsion, rather than just the hydrophilicity of GO. It is known that the residual electrolytes can neutralize the charges on the sheets, destabilizing the resulting dispersions [38]. However, even under the presence of coagulant CTAB, zeta potential slightly became less negative ($\zeta = \sim -40$). It is accepted that zeta potential values more negative than $-30 \, \text{mV}$ is generally considered to represent sufficient mutual repulsion to ensure the

stability of dispersion [39]. Thus, the stability of the re-dispersed GO-CTAB solution is approved. Figure 6(b) indicates the relationship between zeta potential and different pH values. The pH = 1.87 (SGO) and pH = 1.57 (SGO) represent the pristine GO gel solutions and the remaining points are pH-adjusted solutions. Unlike what was expected, there is no distinct trend between zeta potentials and pH values. Huge negative values of pristine LGO and SGO solution might come from the sulfuric acid residue by Hummers' method that is usually used to produce GO from Graphite initially. The photo image in figure 6(c) reveals the gradual color changes from brown to black especially from pH = 7 to 8 for SGO. LGO does not exhibit dramatic color change, but rather a gradual color change.

The macroscopic structure of GO in the form of powder or fiber is observed in the XRD patterns (figure 7). The detailed information of the main peaks (table 1) reveals how the basal graphitic planes are stacked.

The SGO and LGO powders made from gel indicated sharp diffraction peaks at 2θ position of 11.10° and 9.92° , corresponding to the interlayer spacing of intercalated GO planes of 7.96 Å and 8.91 Å, respectively. After the wetspinning process of GO into fibers using CTAB as a coagulation agent, the peaks shift toward the left which corresponds to enlarged d-spacing. The increase in d-spacing may be due to some CTAB molecules intercalating between the GO layers. On the other hand, if using NaOH as the coagulation agent, the layer-by-layer distance does not considerably change. This might be due to sodium hydroxide being small and highly soluble in water. Not many sodium hydroxide molecules participate in intercalating between layers.

Hence, the crystalline structure does not change before and after GO-NaOH fiber formation. It should be noted that although there is a difference in the degree of interlayer spacing for both GO-CTAB and GO-NaOH fibers, the intercalated structure of GO layers are preserved after fiber formation without significant re-stacking, which would have caused the disappearance of the XRD peak associated with intercalation at $2\theta = \sim 10^{\circ}$. This suggests that re-dispersion

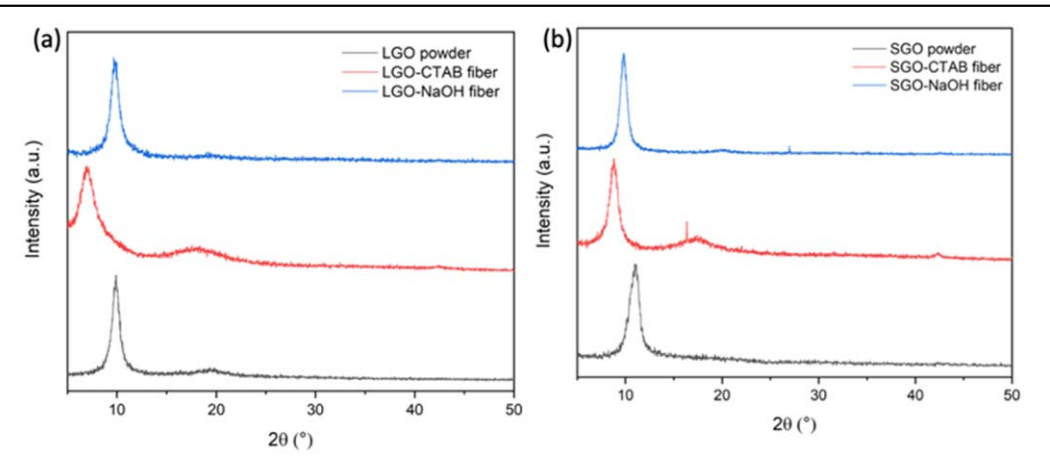


Figure 7. XRD diagrams for (a) LGO and (b) SGO of pristine powders and fibers using different coagulants. Pristine GO solutions were frozen overnight and then ground into powders before conducting XRD.

Table 1. And peak analysis of the inglest intensity peak.					
	2θ (°)	d-spacing (A°)	FWHM (°)	Crystalline domain Size (nm)	Number of layers
SGO	11.10	7.96	1.13	14.12	17.74
SGO-CTAB	8.79	10.05	1.02	15.62	15.54
SGO-NaOH	9.84	8.98	0.78	20.44	22.76
LGO	9.92	8.91	0.74	21.54	24.19
LGO-CTAB	7.04	12.54	1.21	13.15	10.49
LGO-NaOH	9.68	9.13	0.85	18.75	20.55

Table 1. XRD peak analysis of the highest intensity peak

of these GO fibers can offer a solution of GO with an intercalated state. Meanwhile, the Scherrer equation is used to calculate the mean of the crystalline domain of the powdered LGO/SGO and the GO-CTAB fiber. The number of crystalline layers is obtained considering the mean size of the crystalline domain and interlayer spacing. For LGO and SGO, the pristine GO solutions and GO-NaOH fibers have a similar number of crystalline layers. GO-CTAB has only about 10 layers for both cases, which can be attributed to the process of ultrasonication and the possibility of the pristine crystalline structures being ruined. Interestingly, there are small but broad peaks for both GO-CTAB cases at $2\theta = \sim 18^{\circ}$ but cannot be seen in pristine GO nor GO-NaOH curves. This might be because the formation of the secondary structure due to folding or bending of intercalated-CTAB GO sheets or extra random GO sheet wrinkles and crumples caused by CTAB-facilitated self-assembly process.

The FT-IR spectra in figure 8(a), illustrate the LGO and SGO solutions and GO-CTAB fibers has oxygenated functional groups in its graphitic sheets: carboxyl (COO), carbonyl (-C=O), aliphatic C-H, and hydroxyl (-OH) groups on the graphene sheet basal plane and edges.

There are six main peaks centered at 970, 1040, 1622, 1730, 2852, 2924, and 3220 cm⁻¹. The peaks at 1040 and 1622 cm⁻¹ denote the presence of C–O–C stretching vibration and stretching of the unoxidized conjugated graphitic domain (C=C). The peak at 1730 cm⁻¹ arises from the stretching vibration of C=O group. The two small peaks at 2852 and 2924 cm⁻¹ correspond to symmetric and asymmetric aliphatic C–H stretching. The

broad peak at 3220–3400 cm⁻¹ indicates the presence of OH stretching in carboxyl (COOH) and hydroxyl (–OH) groups from the GO edges or the deposited moisture from the air [40, 41]. FT-IR absorption patterns were similar in figure 8(a). This demonstrates that GO-CTAB fibers preserved the functional groups (hydroxyl and carboxyl group) of the initial GO dispersion, whereas the peak at 1730 in the GO solutions has reduced in intensity when interacted with NaOH and it appeared as a shoulder. Instead the 1622 cm⁻¹ peak was stronger than the original solution. The peaks at 2852 and 2924 cm⁻¹ disappeared in the GO-NaOH fibers in 8 (b) presumably due to being overlapped by the OH peak which has broadened.

3.2. Liquid crystallinity

To investigate the preservation of the liquid crystal state in the re-dispersed GO fiber solutions, polarized optical microscopy (POM) was applied. Jalili et al have shown the direct relationship between the GO lateral size and concentration on one hand, and liquid crystallinity of the fiber on the other hand [31]. Here we looked at the effect of the lateral GO sheet size on the re-distributed GO dispersions to investigate the preservation of liquid crystallinity.

Figure 9 shows POM images of the pristine GO and the solution after re-dispersing the GO powders into water. Figure 9(a) indicates polarized light hardly passing through the pristine SGO sample, while it changes when rotating the polarizer by 50 degrees, denoted in figure 9(b). This suggests highly ordered GO nematic domains, evidenced by the spreading Schlieren textures [42]. A similar birefringence

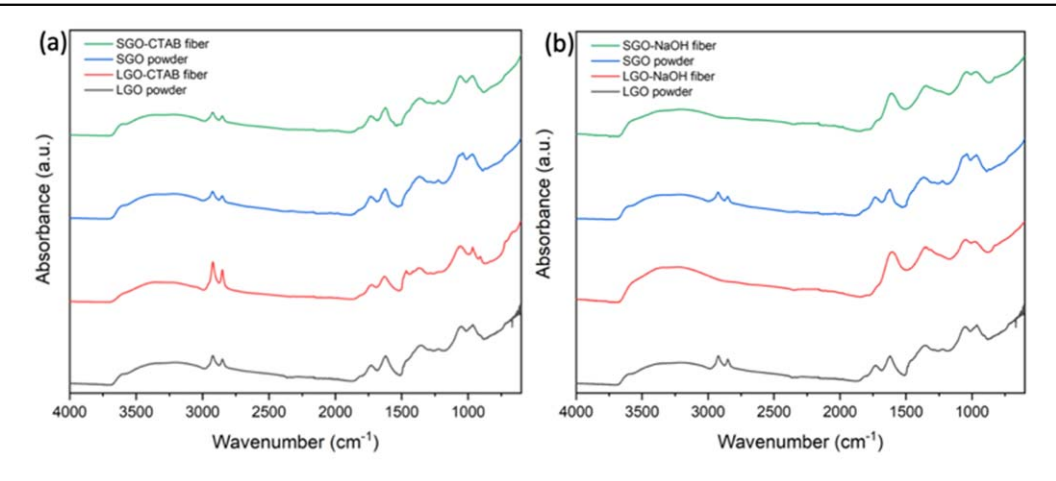


Figure 8. FT-IR spectra for (a) LGO, SGO powders and their fibers obtained after coagulation with CTAB and (b) LGO, SGO powder and their fibers obtained after coagulation with NaOH. Pristine GO solutions were frozen overnight and then ground into powders before conducting FT-IR.

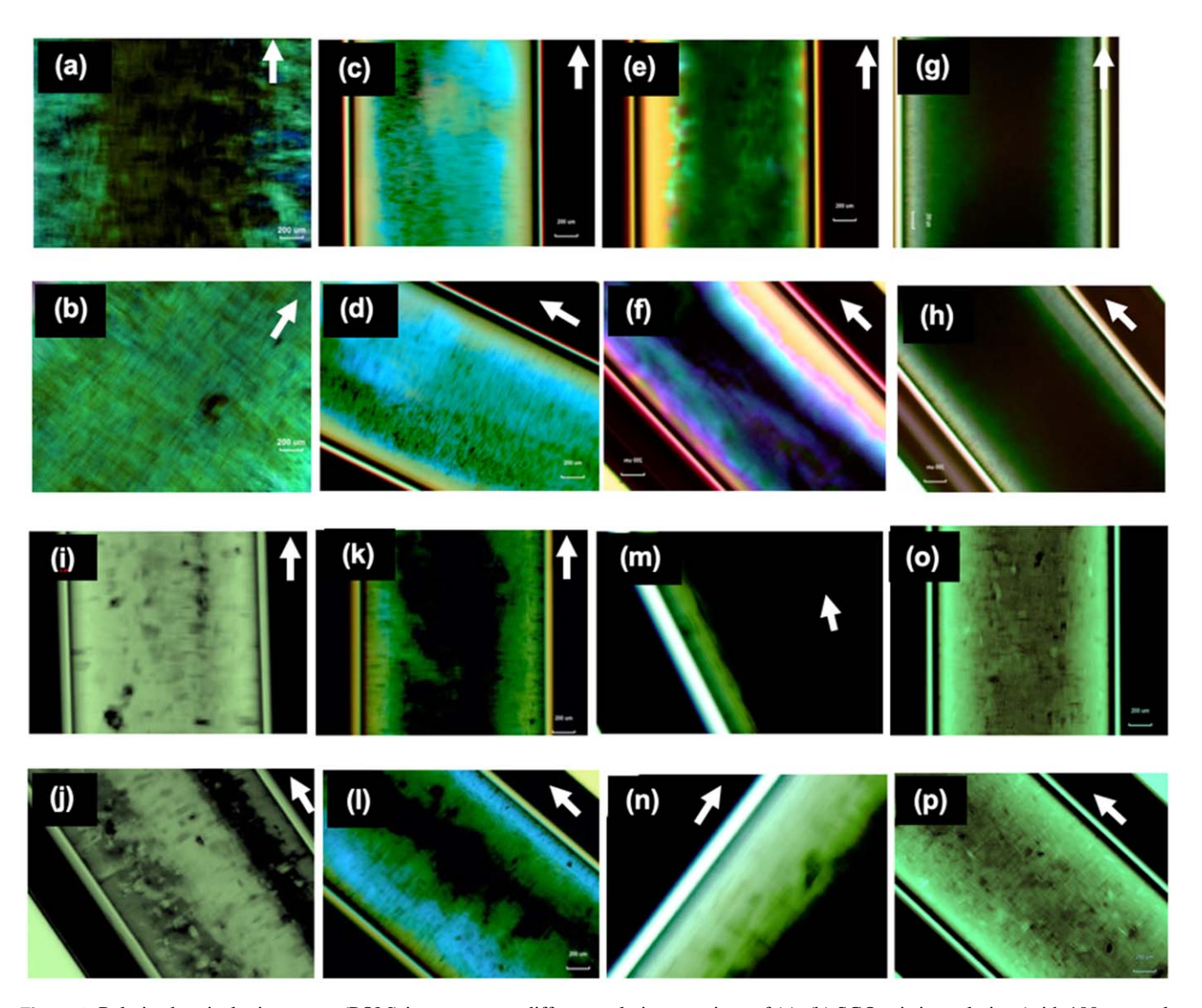


Figure 9. Polarized optical microscopy (POM) images at two different polarizer rotations of (a), (b) SGO pristine solution (with $100 \mu m$ scale bar), (c), (d) SGO-CTAB, (e), (f) SGO-NaOH, (g), (h) SGO-TBAB fiber re-dispersion solution, (i), (j) LGO pristine solution, (k), (l) LGO-CTAB, (m), (n) LGO-NaOH, and (o), (p) LGO-TBAB fiber re-dispersion solution. The GO dispersion samples (2 wt.%) were placed in capillary tubes. The scale bars are $50 \mu m$ for a and b, and $200 \mu m$ for the rest.

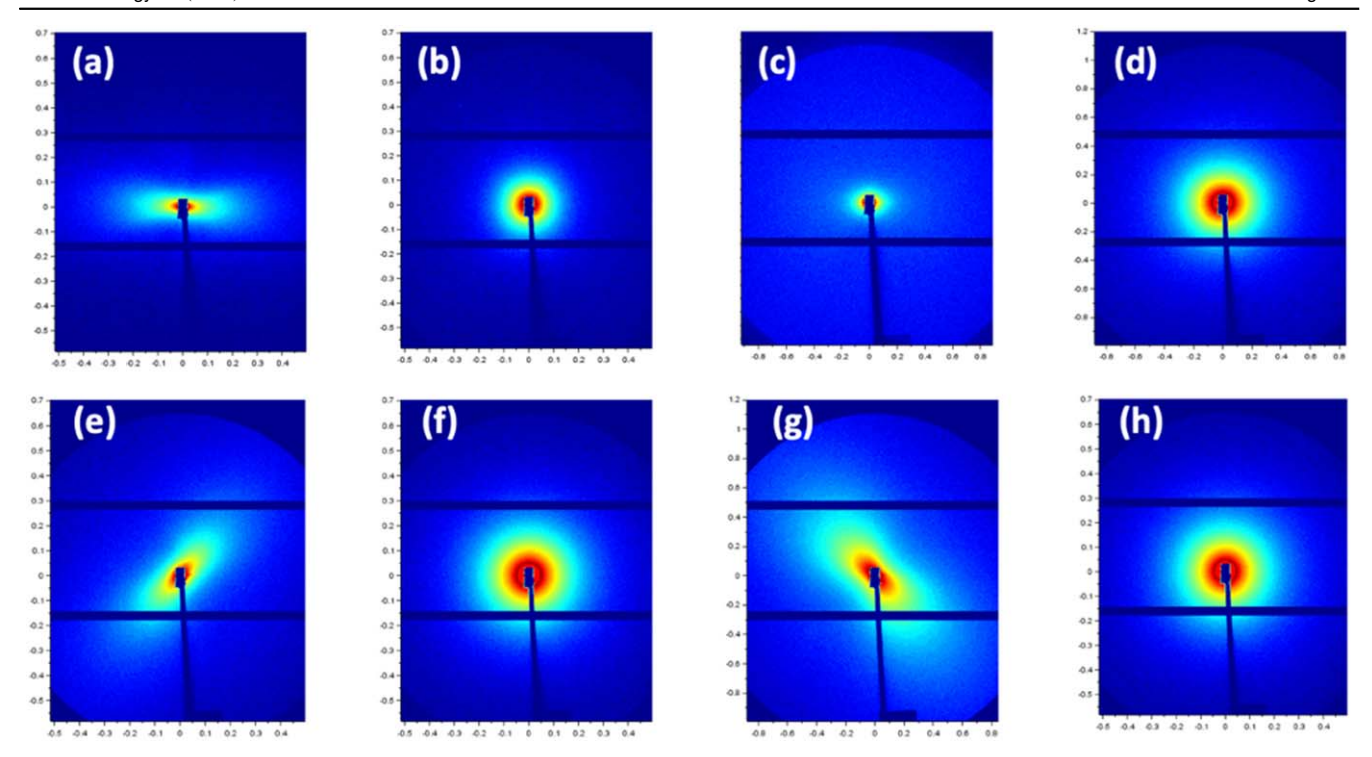


Figure 10. SAXS 2D images of (a) pristine SGO solution and re-dispersed solutions of (b) SGO-CTAB fibers, (c) SGO-NaOH fibers, (d) SGO-TBAB fibers, (e) pristine LGO solution, and re-dispersed solution of (f) LGO-CTAB fibers, (g) LGO-NaOH fibers, and (h) LGO-TBAB fibers. The GO dispersion samples were all at 2 wt.% concentration and were placed in glass capillary tubes.

phenomenon is observed for LGO pristine solutions, as shown in figures 9(i) and (j). However, the GO-CTAB fiber re-dispersed solution does not display birefringence clearly, i.e. no clear differences between. Figures 9(c) and (d) or (k) and (1). A possible reason is that GO sheets aggregate into large particles and the aspect ratio is drastically decreased. The decrease of the aspect ratio and the effect of GO aggregation is proved by the Keyence confocal laser profilometer shown in figure S3. According to Onsager's theory, only above a certain value of aspect ratio liquid crystals in the dispersion can be formed [43]. The challenge is how to exfoliate GO sheets back to their original state. The GO-TBAB (Tetra-n-butylammonium bromide) revealed similar behavior as is shown in figures 9(g) and (h) or (o) and (p). GO-NaOH fiber, on the other hand, referred to as figures 9(e), (f), (m), and (n), showed the clear birefringence behavior at different polarizer rotations. This is because NaOH modified GO sheets with more negatively charged carboxyl groups (-COO⁻) which increased the electrostatics repulsion leading to better redispersion and preventing sheets from aggregation as opposed to in CTAB. Therefore, more exfoliated and transparent GO sheets were preserved. To conclude, both LGO and SGO perform the same way: CTAB makes GO sheets aggregate, while NaOH helps the GO particles recover the liquid crystal state after re-dispersion.

While polarized OM shows the liquid crystal evidence qualitatively, SAXS studies further revealed structural information of GO dispersions. SAXS analysis results are summarized in figure 10. Xu and Gao have previously shown that GO sheets can exhibit nematic liquid crystallinity at mass concentrations higher than 0.5%. They observed a gradual

transition from blank diffusive to elliptical diffusive pattern and then to elliptical pattern by increasing the content of GO [34].

In our case, consistent with POM results, GO-NaOH dispersions of SGO and LGO (c) and (g) exhibited similar nematic crystallinity to the pristine SGO and LGO solutions (a) and (e), indicating the GO fibers that were spun in NaOH, recuperated their ordered liquid crystal structure after redispersion in water. It is worth noting that the elliptical pattern of SGO-NaOH has a larger axial ratio than LGO-NaOH presumably due to larger aspect ratio in SGO sheets. Again, GO-CTAB (b) and (f) and GO-TBAB (d) and (h) in both SGO and LGO cases did not exhibit any anisotropic ordered structure. In summary, the GO-NaOH re-dispersions revealed a nematic phase crystallinity similar to the original GO solutions while GO-CTAB and GO-TBAB did not exhibit the ordered structures at the 2 wt.% concentration.

While polarized OM shows the liquid crystal evidence qualitatively, SAXS studies further revealed structural information of GO dispersions. SAXS analysis results are summarized in figure 10. Xu and Gao have previously shown that GO sheets can exhibit nematic liquid crystallinity at mass concentrations higher than 0.5%. They observed a gradual transition from blank diffusive to elliptical diffusive pattern and then to elliptical pattern by increasing the content of GO [34]. In our case, consistent with POM results, GO-NaOH dispersions of SGO and LGO (c) and (g) exhibited similar nematic crystallinity to the pristine SGO and LGO solutions (a) and (e), indicating the GO fibers that were spun in NaOH, recuperated their ordered liquid crystal structure after redispersion in water. The anisotropic shape in some of the SAXS

patterns appears to be due to a combination of particle form factors and the liquid crystalline orientation of the GO platelets [44] The capillaries were mounted vertically for the measurements. Both SGO and LGO platelets in the pristine solution show a strong preferential orientation with their surface normals aligned along the long axis of the scattering patterns (panels (a) and (e)). The redispersed SGO and LGO platelets spun with CTAB and TBAB appear to have isotropic ordering. In the case of NaOH, SGO particles are mostly isotropic (panel (c)), while LGO particles show again a strong orientation (panel (g)). For LGO particles, the preferential orientation does not appear correlated with the capillary orientation, which may be an artifact of the specific filling conditions.

4. Conclusion

Due to the dramatic mass reduction, the self-assembled GO fibers are a much easier and of a lower-cost method for handling and transportation compared to conventional GO solutions with huge volume/mass of water. In addition, the water-based wet-spinning process is easy to scale up. We demonstrated that the dispersed state of GO solution after redispersing the fabricated GO fibers can be tailored by the selection of coagulant during wet spinning.

A conclusion is drawn that after transforming GO water dispersion into fibers, GO solid could be extracted from a bulky gel without considerably altering the physical and chemical structures such as restacking. With different coagulation agents, different purposes can be fulfilled. Sodium hydroxide is good at maintaining liquid crystallinity and preventing re-stacking, whereas CTAB is good at retaining chemical properties. This facile method based on assembling GO into fibers, followed by re-dispersion in water is very promising for cost-effective GO transportation, as it easily avoids the transportation of the huge volume of water in current GO solution handling. For instance, transportation of GO as solid fibers with a bulk density of 0.25 g cm⁻³ can reduce the transportation volume by 90% compared to the 2.5 wt% GO solution.

Acknowledgments

This work made use of the Cornell Center of Materials Research (CCMR) Shared Facilities, which are supported through NSF MRSEC program (DMR-1719875). This work was also partially supported by JMC Corp. via the CCMR INVEST Program and was supported by the Basic Science Research Program through the National Research Foundation of Korea (NRF), funded by the Ministry of Education (2016R1A6A1A03012069). Beamline ID3B is supported by AFRL award FA8650-19-2-5220.

Data availability statement

All data that support the findings of this study are included within the article (and any supplementary files).

ORCID iDs

Yong Lak Joo https://orcid.org/0000-0002-4646-1625

References

- [1] Niyogi S, Bekyarova E, Itkis M E, McWilliams J L, Hamon M A and Haddon R C 2006 Solution properties of graphite and graphene J. Am. Chem. Soc. 128 7720-1
- [2] MSE supplies (https://msesupplies.com/products/graphene-oxide-water-dispersion-1000-ml-4-mg-graphene-oxide-per-ml-water?variant=33338357071&utm_medium=cpc&utm_source=google&utm_campaign=Google%20Shopping&_vsrefdom=adwords&gclid=CjwKCAiAy9jyBRA6EiwAeclQhB9TfO2eTRGKreifcq2dB6zzIVPmny3ymwBg9p1vf62zHXS2yCzf1BoCfPUQAvD_BwE)
- [3] AlAmer M, Zamani S, Fok K, Satish A, Lim A R and Joo Y L 2020 Facile production of graphenic microsheets and their assembly via water-based, surfactant-aided mechanical deformations ACS Appl. Mater. Interfaces 12 8944–51
- [4] William S, Hummers J and Offeman R E 1958 Preparation of graphitic oxide J. Am. Chem. Soc. 80 1339
- [5] AlAmer M, Lim A R and Joo Y L 2018 Continuous synthesis of structurally uniform graphene oxide materials in a model Taylor-Couette flow reactor *Ind. Eng. Chem. Res.* 58 1167-76
- [6] Kumar R et al 2019 Recent progress in the synthesis of graphene and derived materials for next generation electrodes of high performance lithium ion batteries Prog. Energy Combust. Sci. 75 100786
- [7] Yu X, Cheng H, Zhang M, Zhao Y, Qu L and Shi G 2017 Graphene-based smart materials Nat. Rev. Mater. 2 1–13
- [8] Becerril H A, Mao J, Liu Z, Stoltenberg R M, Bao Z and Chen Y 2008 Evaluation of solution-processed reduced graphene oxide films as transparent conductors ACS Nano 2 463-70
- [9] Eda G and Chhowalla M 2010 Chemically derived graphene oxide: towards large-area thin-film electronics and optoelectronics Adv. Mater. 22 2392–415
- [10] Eda G, Fanchini G and Chhowalla M 2008 *Nat. Nanotechnol.* 3 270
- [11] Chen D, Tang L and Li J 2010 Graphene-based materials in electrochemistry Chem. Soc. Rev. 39 3157–80
- [12] Dreyer D R, Jia H P and Bielawski C W 2010 Graphene oxide: a convenient carbocatalyst for facilitating oxidation and hydration reactions *Angew. Chem.* 122 6965–8
- [13] Song Y, Qu K, Zhao C, Ren J and Qu X 2010 Graphene oxide: intrinsic peroxidase catalytic activity and its application to glucose detection Adv. Mater. 22 2206–10
- [14] Chen Y, Chen L, Bai H and Li L 2013 Graphene oxide– chitosan composite hydrogels as broad-spectrum adsorbents for water purification *J. Mater. Chem.* A 1 1992–2001
- [15] Hegab H M and Zou L 2015 Graphene oxide-assisted membranes: fabrication and potential applications in desalination and water purification *J. Membr. Sci.* 484 95–106
- [16] Chen L et al 2018 High performance graphene oxide nanofiltration membrane prepared by electrospraying for wastewater purification Carbon 130 487–94

- [17] Hu G et al 2016 3D graphene-foam–reduced-graphene-oxide hybrid nested hierarchical networks for high-performance Li–S batteries Adv. Mater. 28 1603–9
- [18] Zhang B W et al 2019 Targeted synergy between adjacent co atoms on graphene oxide as an efficient new electrocatalyst for Li-CO₂ batteries Adv. Funct. Mater. 29 1904206
- [19] Kumar R *et al* 2020 Heteroatom doped graphene engineering for energy storage and conversion *Mater. Today* **39** 47–65
- [20] Fei L et al 2017 Graphene oxide involved air-controlled electrospray for uniform, fast, instantly dry, and binder-free electrode fabrication ACS Appl. Mater. Interfaces 9 9738–46
- [21] Halim W et al 2018 Directly deposited binder-free sulfur electrode enabled by air-controlled electrospray process ACS Appl. Energy Mater. 2 678–86
- [22] Sohail M et al 2017 Modified and improved Hummer's synthesis of graphene oxide for capacitors applications Modern Electron. Mater. 3 110–6
- [23] Hao Y, Wang S, Shao Y, Wu Y and Miao S 2020 High-energy density Li-ion capacitor with layered SnS₂/reduced graphene oxide anode and BCN nanosheet cathode Adv. Energy Mater. 10 1902836
- [24] Graphene-Supermarket (https://graphene-supermarket.com/ Single-Layer-Graphene-Oxide-Dispersion-in-Water.html)
- [25] Nanografi (https://nanografi.com/graphene/graphene-oxide-water-dispersion-purity-99-5-black-liquid-go-2-0-wt/)
- [26] Seabra A B, Paula A J, de Lima R, Alves O L and Durán N 2014 Nanotoxicity of graphene and graphene oxide *Chem. Res. Toxicol.* 27 159–68
- [27] Clemente Z, Castro V L S, Franqui L S, Silva C A and Martinez D S T 2017 Nanotoxicity of graphene oxide: assessing the influence of oxidation debris in the presence of humic acid *Environ. Pollut.* 225 118–28
- [28] Zeng Z, Yang K and Lin D 2019 The effect of water hardness on the toxicity of graphene oxide to bacteria in synthetic surface waters *Aquatic Toxicol.* 216 105323
- [29] Xu Z, Sun H, Zhao X and Gao C 2013 Ultrastrong fibers assembled from giant graphene oxide sheets Adv. Mater. 25 188–93
- [30] Zamani S et al 2021 Ultralight graphene/graphite hybrid fibers via entirely water-based processes and their application to density-controlled, high performance composites Carbon 173 880-90

- [31] Jalili R *et al* 2013 Scalable one-step wet-spinning of graphene fibers and yarns from liquid crystalline dispersions of graphene oxide: towards multifunctional textiles *Adv. Funct. Mater.* **23** 5345–54
- [32] Dong L, Yang J, Chhowalla M and Loh K P 2017 Synthesis and reduction of large sized graphene oxide sheets *Chem.* Soc. Rev. 46 7306–16
- [33] Lee J H et al 2013 Restacking-inhibited 3D reduced graphene oxide for high performance supercapacitor electrodes ACS Nano 7 9366–74
- [34] Wu H et al 2014 Ph-dependent size, surface chemistry and electrochemical properties of graphene oxide Carbon 67 795
- [35] Kashyap S, Mishra S and Behera S K 2014 Aqueous colloidal stability of graphene oxide and chemically converted graphene J. Nanopart. 2014 640281
- [36] Ghazizadeh S, Duffour P, Skipper N, Billing M and Bai Y 2017 An investigation into the colloidal stability of graphene oxide nano-layers in alite paste *Cement Concr. Res.* 99 116–28
- [37] Whitby R L et al 2011 pH-driven physicochemical conformational changes of single-layer graphene oxide Chem. Commun. 47 9645–7
- [38] Wijesena R N, Tissera N D, Rathnayaka V, de Silva R M and de Silva K N 2020 Colloidal stability of chitin nanofibers in aqueous systems: effect of pH, ionic strength, temperature & concentration *Carbohydrate Polym.* 235 116024
- [39] Xu R, Wu C and Xu H 2007 Particle size and zeta potential of carbon black in liquid media Carbon 45 2806–9
- [40] Hurst J M, Li L and Liu H 2018 Adventitious hydrocarbons and the graphite-water interface Carbon 134 464–9
- [41] Pfaffeneder-Kmen M, Casas I F, Naghilou A, Trettenhahn G and Kautek W 2017 A multivariate curve resolution evaluation of an in situ ATR-FTIR spectroscopy investigation of the electrochemical reduction of graphene oxide Electrochim. Acta 255 160-7
- [42] Xu Z and Gao C 2011 Aqueous liquid crystals of graphene oxide Acs Nano 5 2908–15
- [43] Guo F, Kim F, Han T H, Shenoy V B, Huang J and Hurt R H 2011 Hydration-responsive folding and unfolding in graphene oxide liquid crystal phases Acs Nano 5 8019–25
- [44] Lemaire B, Panine P, Gabriel J and Davidson P 2002 The measurement by SAXS of the nematic order parameter of laponite gels *Europhys. Lett.* 59 55